Human Molecular Genetics, 2022, Vol. 31, No. 5 692–704

https://doi.org/10.1093/hmg/ddab282
Advance Access Publication Date: 24 September 2021
General Article

GENERAL ARTICLE

Enhanced glycolysis and GSK3 inactivation promote brain metabolic adaptations following neuronal mitochondrial stress

Sofia Garcia‡, Amy Saldana-Caboverde‡, Mir Anwar, Ami Pravinkant Raval, Nadee Nissanka, Milena Pinto, Carlos Torres Moraes*,† and Francisca Diaz§

Department of Neurology, University of Miami Miller School of Medicine, Miami, FL 33136, USA

*To whom correspondence should be addressed at: 1420 NW 9th Ave, Neurology Research Building, Room 230B, Miami, FL 33136, USA. Tel: +1 3052435858; Fax: +1 3052436955; Email: cmoraes@med.miami.edu

Abstract

We analyzed early brain metabolic adaptations in response to mitochondrial dysfunction in a mouse model of mitochondrial encephalopathy with complex IV deficiency [neuron-specific COX10 knockout (KO)]. In this mouse model, the onset of the mitochondrial defect did not coincide with immediate cell death, suggesting early adaptive metabolic responses to compensate for the energetic deficit. Metabolomic analysis in the KO mice revealed increased levels of glycolytic and pentose phosphate pathway intermediates, amino acids and lysolipids. Glycolysis was modulated by enhanced activity of glycolytic enzymes, and not by their overexpression, suggesting the importance of post-translational modifications in the adaptive response. Glycogen synthase kinase 3 inactivation was the most upstream regulation identified, implying that it is a key event in this adaptive mechanism. Because neurons are thought not to rely on glycolysis for adenosine triphosphate production in normal conditions, our results indicate that neurons still maintain their ability to upregulate this pathway when under mitochondrial respiration stress.

Introduction

The oxidative phosphorylation (OXPHOS) system, located in the inner mitochondrial membrane, is composed of five multi-subunit complexes that transfer electrons from nicotinamide adenine dinucleotide (reduced) (NADH) and $FADH_2$ to molecular oxygen. This electron transfer is coupled to the production of adenosine triphosphate (ATP). Disorders that affect the function of the OXPHOS system have been traditionally referred to as mitochondrial diseases, which have a wide range of clinical presentations, are commonly multisystemic and have an estimated frequency of 1/4300 (1). Despite remarkable progress in the last 5–10 years in understanding the mechanisms of disease using patient-derived cell lines and animal models [reviewed in (2,3)], to date, there is no cure or effective treatment for mitochondrial diseases. Impaired mitochondrial function has also been associated with numerous neurodegenerative diseases, with ischemia caused by stroke or cardiac arrest and with normal aging (4).

To understand the basis of the pathological mechanisms of mitochondrial diseases, we created a mitochondria encephalopathy mouse model with cytochrome c oxidase (COX) deficiency. This mouse animal model was produced by the ablation of the *Cox10* gene in neurons (5,6). COX or complex IV (CIV) is the terminal enzyme of the electron transport chain, which transfers

†Carlos Torres Moraes, http://orcid.org/0000-0002-8077-7092
‡Contributed equally.
§Deceased 5 March 2021.
Received: July 21, 2021. **Revised:** September 10, 2021. **Accepted:** September 17, 2021

electrons from cytochrome c to oxygen. The biosynthesis of this multi-subunit complex requires >30 different assembly factors (7). One of these factors is COX10, a farnesyl transferase that participates in heme *a* biosynthesis (8). Heme *a* is a prosthetic group unique to the cytochrome c oxidase subunit 1 (Cox1) subunit of CIV. Cox1 is the first subunit in the assembly line of CIV and, without heme *a*, Cox1 is unstable, degraded and CIV is not assembled (9). Mutations in COX10 in humans cause disease and premature death with various pathologies, including leukodystrophy, tubulopathy, anemia, Leigh syndrome (LS), sensorineural deafness and fatal infantile hypertrophic cardiomyopathy (10–12).

We previously showed that in neuron-specific COX10 knockout (KO) (nKO) mice, the onset of the mitochondrial defect did not coincide with early cell death, suggesting adaptive mechanisms to maintain neuronal survival (5) In the present study, we investigated the metabolic consequences of the mitochondrial defect in the central nervous system (CNS) of the COX10 nKO mice and found significant increases in brain glucose uptake, glycolytic and pentose phosphate pathway (PPP) intermediates, lysolipids and certain amino acids. Interestingly, the increased glycolysis was not accompanied by an increase in the steady-state level of glycolytic enzymes, suggesting that post-translational modifications participate in the adaptive response. We identified changes in the activity of glycogen synthase kinase 3 (GSK3) that might control the downstream metabolic changes observed and might promote neuronal survival.

Understanding these early adaptive mechanisms will allow for the identification of new therapeutic targets for the treatment of mitochondrial diseases and other neurodegenerative disorders associated with mitochondrial dysfunction.

Results

Global metabolomic analysis of COX10 nKO cortical and hippocampal tissue

Deletion of COX10 in adult forebrain neurons caused a progressive mitochondrial encephalopathy (5) Surprisingly, the neurons in the COX10 nKO mice survived for an extended period of time after the onset of the mitochondrial defect (assessed by significant decrease in CIV activity). The onset of the mitochondrial defect was observed in 1–2-month-old mice when CIV activity in the COX10 nKO was approximately 70% (in hippocampus) and 75% (in cortex) of controls. As the disease progressed, CIV activity declined to about 23% (in hippocampus) and to 33% (in cortex) by 4 months (5). Because these homogenates contain other cell types, it is safe to assume that the COX defect in neurons was much more severe than the homogenate numbers showed. The onset of neurodegeneration was observed only at 4 months when terminal deoxynucleotidyl transferase dUTP nick-end labeling-positive cells were found in specific regions of the brain and, later on, developed into a severe cortical atrophy (5).

Since the mitochondrial defect did not coincide with immediate cell death, we decided to investigate the metabolic changes and potential early adaptive responses, which could promote neuronal survival. To characterize early adaptive responses, we analyzed cortex and hippocampus of 2- and 3-month-old mice through a global, unbiased metabolomic and proteomic approach.

The global metabolomic profile of control and COX10 nKO mice was performed using three platforms [liquid chromatography (LC)/mass spectrometry (MS); LC/MS/MS and gas chromatography (GC)/MS]. In cortex, a total of 248 metabolites were identified. Out of those metabolites, only 18 were significantly altered at 2 months and 57 at 3 months (Supplemental Material, Fig. S1 and Supplemental Material, Table S1). Similar analysis in hippocampus revealed that out of 183 identified metabolites, only 14 significantly changed at 2 months and 58 at 3 months (Fig. 1 and Supplemental Material, Table S2). The main changes in metabolites in the COX10 nKO mice compared with controls were observed in pathways related to glucose/energy, amino acids and lipid metabolism (Fig. 1).

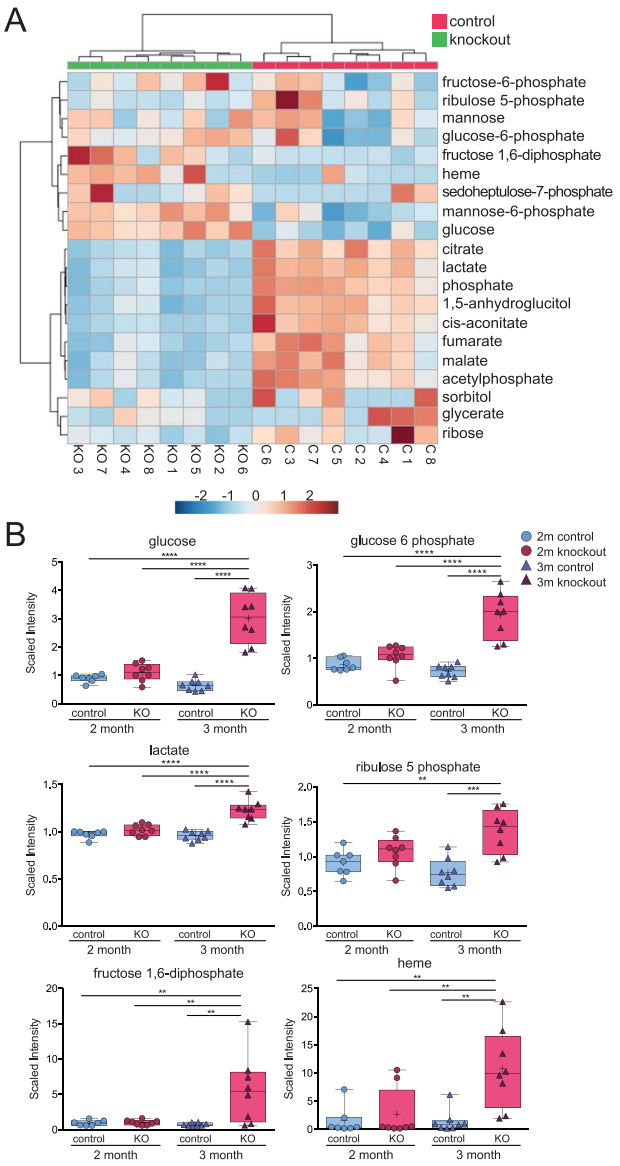

Figure 1. Metabolomic profile of glycolysis, pentose phosphate and TCA cycle pathways in COX10 KO hippocampus. (**A**) The heat map for selected metabolites in the COX10 nKO compared with control mice at 3 months in hippocampus. Red boxes indicate increases, while blue boxes indicate decreases in peak intensity values for metabolites ($n = 8$). Data normalization was done using the median sample value. (**B**) Graphs (box and whiskers plots) show the scaled intensity of selected metabolites of both 2- and 3-month-old mice for hippocampus. Data normalization was done using the raw median value of all samples analyzed per metabolite. Mean value ($n = 7$–8) is represented with a '+' sign; median value is represented by line inside the box; upper and lower quartiles shown above and below of median and maximum and minimum distribution are shown as error bars. (**) indicates significance at $P < 0.01$, (***) indicates significance at $P < 0.001$, (****) indicates significance at $P < 0.0001$.

Increased glycolytic intermediates and glucose uptake in the COX10 nKO mouse

To satisfy the energetic demands of the cell, mitochondrial dysfunction could lead to an increase in glycolysis. There was a significant increase in the levels of glucose, glucose 6-phosphate and fructose-1,6-diphosphate in the brains of 3-month-old COX10 nKO when compared with control mice; however, no significant changes in these carbohydrates were observed at 2 months (Fig. 1). The increase of these metabolites suggests that glycolysis is upregulated in the CNS of 3-month-old COX10 nKO (Fig. 1 and Supplemental Material, Fig.S1).

Related to the tricarboxylic acid cycle (TCA) cycle, there was a small but significant increase in the levels of fumarate and malate in hippocampus but not in cortex of the COX10 nKO (Fig. 1 and Supplemental Material, Fig. S1), which is in agreement with a defective electron transport chain. Lactate levels were slightly increased in both hippocampus and cortex (Fig. 1 and Supplemental Material, Fig. S1).

Part of the glucose appears to be directed to the PPP, as indicated by the increase of some intermediates like ribulose 5-phosphate, ribulose, ribose and xylitol (Fig. 1 and Supplemental Material, Fig. S1). The PPP, in its initial steps, shunts glucose-6-phosphate to the production of NADPH and maintains the redox homeostasis through reduced glutathione for detoxification of hydrogen peroxide. Heme accumulation increases at 3 months in cortex and hippocampus, respectively (Fig. 1 and Supplemental Material, Fig. S1) was expected, as the ablation of COX10 causes a block in the heme *a* biosynthetic pathway and accumulation of its precursor. The levels of the cellular antioxidants glutathione and α-tocopherol in the nKO mice are similar to the ones found in control animals, which is in agreement with our previous observations of reduced oxidative stress markers at early ages in the COX10 nKO (5) The complete metabolomics fold change data are shown in Supplemental Material, Tables S1 and S2.

The brain is the major glucose-consuming tissue in the body. To confirm the increased levels of glucose observed by the metabolomic analysis, we determined the overall glucose uptake *in vivo* by using [^{14}C]2-deoxy-glucose (2-DG). This glucose analog enters the cells and is rapidly phosphorylated. Because there is little expression of glucose-6-phosphatases in the brain, the deoxy-glucose-6-phosphate is retained and accumulated inside the cells as it cannot be further metabolized. To assess the 2-DG uptake, mice received an i.p. injection of [^{14}C]2-DG and, after 45 min, the brain was dissected and the frozen brain sections were exposed to film. Figure 2A shows a marked increase in the uptake of radiolabeled [^{14}C]2-DG in the COX10 nKO brain, which is in agreement with the metabolomic data shown in Figure 1. The increased glucose uptake most likely occurred in neurons as they are the cells with the mitochondrial defect. Previous studies investigated the cellular compartment that uptakes glucose in the brain. Using near-infrared-labeled 2-DG (2DG-IR) and two-photon microscopy, Lundgaard and collaborators (13) demonstrated that 2DG-IR was preferentially taken up by neurons and not by astrocytes *in vivo*. These findings are in agreement with our observations.

Increased enzymatic activity of some glycolytic enzymes in the COX10 nKO mouse

Since we observed increased levels of glucose and other glycolytic and PPP intermediates in both cortex and hippocampus, and increased uptake of 2-DG in the COX deficient brains, we decided to analyze the enzymatic activity of key regulatory enzymes of the glycolytic pathway in cortex homogenates. Glycolysis is controlled mainly by three regulatory enzymes: hexokinase (HK), phosphofructokinase (PFK) and pyruvate kinase (PK). HK is the first enzyme of the glycolysis that catalyzes the phosphorylation of glucose into glucose-6-phosphate and is regulated by end-product inhibition. PFK catalyzes the phosphorylation of fructose-6-phosphate into fructose-1,6-diphosphate and is allosterically regulated by ATP and fructose-2,6-biphosphate. PK catalyzes the conversion of phosphoenol pyruvate to pyruvate and is also allosterically regulated by ATP, alanine and fructose-1,6-biphosphate.

Figure 2B shows a significant increase in the enzymatic activity of HK in the nKO mice when compared with control animals. An increase in the enzymatic activity of PK was observed, although only statistically significant at 4 months, which is consistent with increases in the allosteric regulators. Both alanine and fructose-1,6-biphosphate were significantly increased in cortex and hippocampus of 3-month-old nKO mice (Fig. 1 and Supplemental Material, Fig. S1 and Supplemental Material, Tables S1 and S2).

The enzymatic activity of PFK and lactate dehydrogenase (LDH) were not altered in cortex homogenates (Fig. 2B). LDH catalyzes the reversible conversion of pyruvate to lactate. There are two genes: LDHA (muscle isoform) and LDHB (heart isoform), and these isoforms are combined to form a homo- or hetero-tetramer. We analyzed the five LDH isoforms in cortex from control and nKO mice and observed a significant increase only in the levels of LDH5 and LDH4 (Supplemental Material, Fig. S2), indicating higher LDHA expression. These results are consistent with increased lactate observed in the metabolomics analysis (Fig. 1).

Lactate moves through cells in the brain via monocarboxylate transporters (MCTs). MCT1 and MCT2 are the main transporters of lactate in astrocytes and in neurons, respectively. MCT1 is developmentally regulated in the rodent brain and its expression increases in astrocytes and decreases in neurons with development (14,15). MCTs could be regulated by diet/substrate availability or by neuronal activity (16,17). MCT2 but not MCT1 expression is controlled at the transcriptional level by noradrenaline stimulation, which can regulate brain energy metabolism by enhancing lactate production during synaptic activity (17). Supplemental Material, Figure S3 shows a significant increase in the levels of MCT2 in cortex homogenates, suggesting that the increased lactate is produced by neurons, which is consistent with the results in Figure 1 and Supplemental Material, Figure S1.

Steady-state level of glycolytic enzymes are not significantly altered

To determine if the increase in the glycolytic pathway observed in the COX10 nKO mice was owing to changes in the expression level of enzymes, we analyzed the steady-state levels of several glycolytic enzymes by western blot (Supplemental Material, Fig. S4A). No obvious differences were observed between control and KO mice in hexokinase 1 (HK1), PK [pyruvate kinase, muscle isoform 2 (PKM2), muscle isoform-2 highly expressed in brain], pyruvate dehydrogenase kinase 1 (PDK1), phosphofructokinase isoform 2 (PFK2) and glyceraldehyde 3 phosphate dehydrogenase (GAPDH) levels at different ages in cortex homogenates (Supplemental Material, Fig. S4A). A more detailed analysis of 2- and 3-month-old mice still did not show significant differences between control and nKO mice for all glycolytic enzymes tested in cortex homogenates (Supplemental Material, Fig. S4B and C).

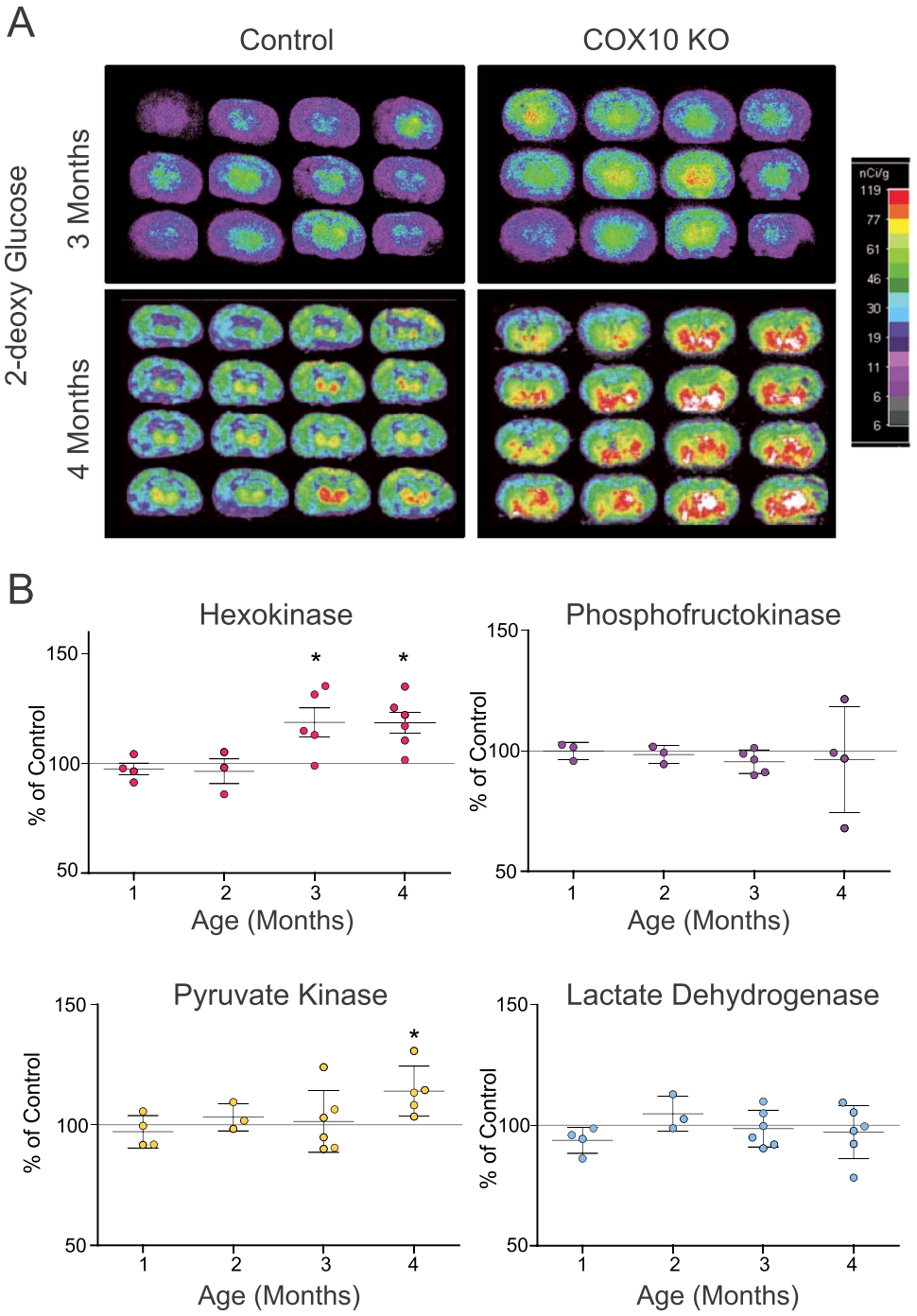

Figure 2. Glucose uptake and enzymatic activity of glycolytic enzymes in COX10 nKO. **(A)** Brain 2-deoxyglucose uptake in control and nKO mice: brain sections were exposed to autoradiography and were digitalized and intensities are shown in pseudocolors. COX10 nKO mice showed increased glucose uptake in brain compared with control mice. **(B)** Enzymatic activity of key regulatory enzymes in glycolysis was determined spectrophotometrically and expressed as percentage of controls (horizontal line at 100% is shown in the graphs). Symbols represent individual nKO mice and lines represent mean (middle line) and standard deviation ($n = 3$–6). (*) indicates statistical significance $P < 0.05$.

Analysis of hippocampus homogenates revealed a significant decrease in the levels of PKM2 and a significant increase in the PDH only at 2 months (Supplemental Material, Fig. S4C). Two forms of PKM2 have been described, a dimeric less active form and a tetrameric highly active form (18). The phosphorylation in Tyr105 of PKM2 disrupts the tetramer (19). In contrast, allosteric regulation by fructose 1,6-diphostate or serine facilitates the formation of the tetrameric form of PKM2 (20). Determination of the ratio between pPKM2/PKM2 or dimeric/tetrameric forms to estimate activity state of PKM2 showed no significant increase of this enzyme in the nKO mice (Supplemental Material, Fig. S4C). Interestingly, the increased levels of glycolytic metabolites (Fig. 1) increased glucose uptake and enzymatic activity of HK and PK (Fig. 2), and the lack of significant differences on the

steady-state levels of glycolytic enzymes (Supplemental Material, Fig. S4) suggest that the regulation of the glycolysis pathway in the COX10 nKO might be achieved by allosteric regulations or by post-translational modifications.

Increased glycolysis preserves ATP levels in COX10 nKO

One of the hallmarks of mitochondrial diseases is the reduced ATP production (21). Interestingly, the global metabolomic analysis did not reveal significant differences in the levels of ATP between the control and nKO mice. The adenosine monophosphate (AMP) levels were significantly decreased in cortex and hippocampus. ADP was increased in nKO mice at 3 months in the cortex but was not detected in the hippocampus (Supplemental Material, Fig. S5 and Supplemental Material, Tables S1 and S2). These results suggest that enhanced glycolysis was most likely responsible for the maintenance of controlling ATP levels in the COX10 nKO mice, although increased purine biosynthesis could also play a role.

Global protein expression analysis using DIGE and phosphoproteome

To investigate the mechanisms of increased glycolysis, we decided to examine the global proteome and phosphoproteome by differential gel electrophoresis (DIGE). Hippocampal proteins from 2- and 3-month-old control and COX10 nKO mice were labeled with Cy3 or Cy5, respectively, mixed and then separated by two-dimensional polyacrylamide gel electrophoresis. Figure 3A shows a representative image of the DIGE showing the control (green) and COX10 nKO (red) labeled proteins. Analysis of fluorescence intensities of the spots, using Image QuantTL and DeCyder software (GE Healthcare), revealed statistically significant changes on 12 and 15 of the detected proteins at 2 and 3 months respectively, with fold change differences $\geq$1.3 (Supplemental Material, Table S3). Spots corresponding to significant changes are indicated with circles in Figure 3A.

Selected spots were excised from the gel and were subjected to MS for identification (Supplemental Material, Table S3). Among the proteins increased in the nKO, there were: glial fibrillary acidic protein (GFAP, 2.2-fold); glyoxylate reductase/hydroxypyruvate reductase (GRHPR, 1.23-fold increase); glyceraldehyde 3 phosphate dehydrogenase (GAPDH, 2.02-fold increase); cytochrome c1 (1.38-fold decrease); COX subunit 5a (Cox5a, 1.65-fold decrease) and hemoglobin α and β (both decreased at 2 months and increased at 3 months). Increased levels of GFAP indicated glial activation in the COX10 nKO mice. We have reported gliosis in this mouse model with a clear difference in the levels of GFAP between control and nKO mice at 4 months (5). An increase in the levels of GAPDH in the nKO mice detected by DIGE is consistent with increased glycolysis, although we were not able to detect this by regular western blot, possibly because the latter is less sensitive than DIGE. The increase of hemoglobin α and β in the nKO mice at 3 months could be related to increased vascularization/blood flow of the tissue to provided substrate for an increased glycolytic rate. Interestingly, reports by several groups indicated that hemoglobin is also expressed in neurons and oligodendrocytes, although its intracellular function remains elusive (22–24). Whether the hemoglobin detected in the 2D-gels is intracellular or if it is owing to trace amounts of blood in the perfused tissue is unknown. GRHPR converts hydroxypyruvate to glycerate, which can be used as an energy source as it can be converted to glucose by other enzymes. The decrease in the levels of Cox5a, one of the subunits of COX, is consistent with the COX10 deletion in the nKO mouse.

The global proteome analysis of the COX10 nKO by DIGE revealed small changes in few proteins, suggesting that there might be a more important role for post-translational modifications in the metabolic reprograming of the COX10 nKO mice. To test this, phosphoproteins were labeled by staining gels with ProQ diamond (red) and overlayed with the image of total proteins labeled with Cy5 (green). Circled spots in Figure 3B and C show proteins increased or unique to either the control or the COX10 nKO mice. Again, selected spots were excised and proteins were identified by MS (Supplemental Material, Table S4). Among the identified phosphoproteins unique to the nKO, there were some enzymes involved in carbohydrate metabolism and TCA cycle: GAPDH, glycogen phosphorylase (GP), glucose 1,6-biphosphate synthase, aldolase A, succinate dehydrogenase flavoprotein and acetyl CoA synthetase 2-like.

Phosphorylation of GAPDH increases its activity (25), which is in agreement with the increased glycolysis observed in the COX10 nKO mice. Glucose 1,6-biphosphate synthase produces glucose 1,6-biphosphate by transferring the phosphate group from 1,3-biphosphoglycerate to glucose 1-phosphate. Glucose 1,6-biphosphate regulates glycolysis by activating PFK and PK, regulatory enzymes of the pathway and is also a precursor for the PPP. Aldolase catalyzes the conversion of fructose 1,6-biphosphate to glyceraldehyde 3-phosphate and dihydroxyacetone in the fourth step of glycolysis. GP catalyzes the limiting step in glycogenolysis by releasing glucose 1,6 phosphate from glycogen and its activity is regulated by phosphorylation in Ser14 residue, transforming the phosphorylase b (inactive) into phosphorylase a (active form) (26). The role of phosphorylation in many of the other enzymes has not been described and there are no antibodies specific for phosphorylated forms for further validation. Taken together, the phosphoproteome results are in agreement with increased glycolysis in the COX10 nKO mice and support the relevance of post-translational modifications to regulate this pathway.

Kinases implicated in cell metabolism and survival

To understand the mechanism of the metabolic reprograming with increased glycolysis and the delayed cell death during the mitochondrial defect, we investigated kinases implicated in metabolic regulation and cell survival pathways, such as AMPK and AKT.

Adenosine monophosphate-activated protein kinase (AMPK) acts as a sensor and regulates energy metabolism in response to cellular stress, exercise, hormonal changes and other signals (27). AMKP is a heterotetramer composed of a catalytic α subunit (α1 or α2) and two regulatory β (β1 or β2) and γ (γ1, γ2 or γ3) subunits. Increased AMP/ATP or ADP/ATP ratios can stimulate AMPK by promoting phosphorylation in Thr172 residue in the α subunit [reviewed in (28)]. We analyzed the levels of total and phosphorylated (Thr172) AMPK α-subunit in cortex and hippocampus homogenates of control and nKO mice and observed a significant decrease in the levels of AMPKα in the hippocampus of 2-month-old nKO mice (Supplemental Material, Fig. S6). This difference in the levels of AMPK resulted in a significantly increased ratio of phosphorylated to total AMPKα protein in cortex (Supplemental Material, Fig. S6), suggesting activation of this kinase. To confirm activation of AMPK at 2 months, we also examined the total levels and phosphorylation state of the AMPK substrate acetyl CoA carboxylase (ACC) in Ser79. Again,

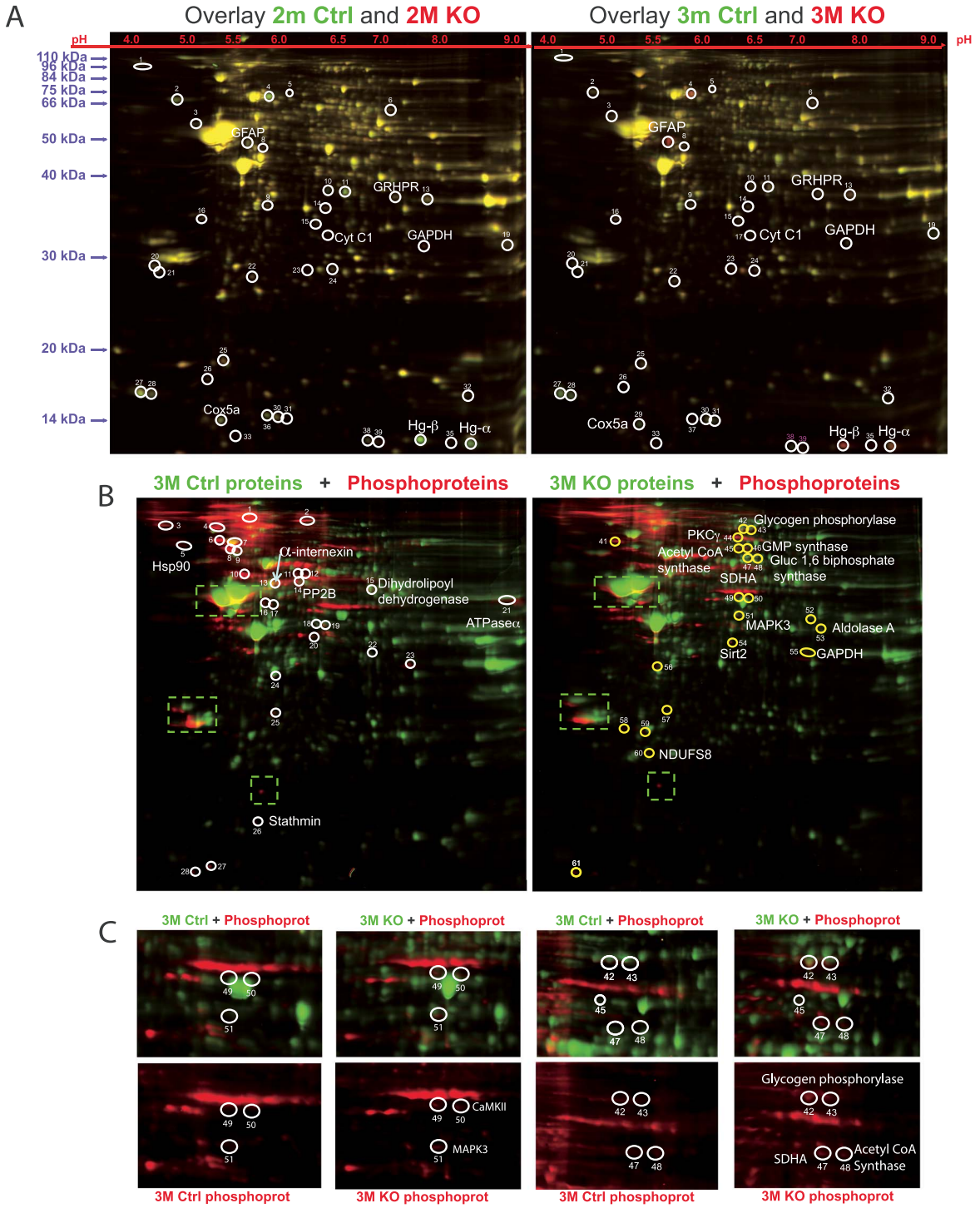

Figure 3. Global- and phospho-proteomics of COX10 nKO by DIGE. (**A**) Proteins from Ctrl and nKO mice at 2 and 3 months were labeled with either cy3 (green) or cy5 (red), respectively, samples were mixed and separated by 2-D gel electrophoresis. Proteins marked with circles represent those with significant different levels. Mass spectrometry of some spots identified GFAP, GRHPR, Cytochroem c1, GAPDH, Cox5a and hemoglobin α and β (Hgα and Hgβ) as differentially expressed in control and COX10 nKO mice. (**B**) Proteins were labeled with Cy3 (green), separated by 2D electrophoresis and phosphoproteins were stained with ProQ diamond (red). Some of spots were excised and proteins identified by mass spectrometry. (**C**) Magnification of some spots on (**B**). Gels in figure are representative images of $n = 3$ per group.

we did not observe changes in pACC (Supplemental Material, Fig. S6). ACC is involved in fatty acid synthesis and its phosphorylation promotes the uptake of fatty acids into the mitochondria (29). These results suggest that either ACC is not an important target of AMPK in the COX10 nKO brain or that the increased pAMPKα/AMPKα ratio was not enough to result in detectable changes in the phosphorylation of ACC in the nKO mice. AMPK is also known to stimulate glycolysis by phosphorylating PFK2 or fructose-2,6-bisphosphatase phosphofructokinase-2 (FBPase-2) which produces fructose-2,6-biphosphate, a potent stimulator of the regulatory enzyme PFK (30). Although we did not examine the phosphorylation levels of PFK2 owing to lack of reliable

antibodies, we did not observe an increase in the enzymatic activity of PFK (Fig. 2B) nor detected fructose-2,6-biphosphate by metabolomics analysis (Supplemental Material, Tables S1 and S2). Taken together, these results suggest that AMPK does not have a major role in the early metabolic adaptation to increase glycolytic flux in the mitochondrial respiration-deficient model.

AKT or protein kinase B (PKB) is a serine/threonine kinase with diverse cellular roles, including the control of metabolism, growth, proliferation, protein synthesis, angiogenesis, migration and cell survival (31). There are three isoforms of this kinase and their activity is regulated mainly by phosphorylation and by various post-translational modifications, including acetylation, glycosylation, ubiquitination and oxidation (32). AKT1 is mainly phosphorylated at Thr308 by phosphoinositide-dependent protein kinase 1 and at Ser473 by mammalian target of rapamycin complex 2 (33,34). The full activation of AKT is reached by phosphorylation of both residues. We examined the phosphorylation state of AKT and observed that there was a significant increase in the ratio of pThr308/total protein in the cortex homogenates of COX10 nKO at 2 months (Fig. 4A and B). Phosphorylation at Thr308 is suggestive of an activation of the phosphoinositol 3 kinase/AKT signaling pathway, which adjusts the metabolic and biosynthetic response to environmental or stress alterations, such as nutrient changes (35,36). However, a significant increase in the pSer473AKT/AKT was observed at 3 months in both cortex and hippocampus. Recently, it was suggested that the ratio of AKT pSer473/pThr308 could be a good indicator of the activity and predictor of substrate specificity in AKT signaling (37). We did not observe differences in the ratio of pSer473/pThr308 of AKT between control and COX10 nKO mice.

One of the targets of AKT implicated in cell metabolism, cell survival and control of apoptosis is GSK3. GSK3 is a constitutively active kinase and its activity is regulated by phosphorylation; when phosphorylated, GSK3 is inactive (38). We analyzed the steady-state levels of GSK3 by western blot using antibodies against the total and phosphorylated forms of both GSK3α and GSK3β (phosphorylated at Ser21 and Ser9, respectively) at different ages (Fig. 4C). Closer analysis shows that, at 1 month, there is a small significant increase in the levels of GSK3α in nKO mice compared with controls, but there were no differences in the GSK3β or in the ratio of phosphorylated to total protein in cortex homogenates (Fig. 4C). Interestingly, at 2 months, there was a change in the phosphorylation of the kinase and we observed a significant increase in the levels of phospho-GSK3β (pGSK3β) and in the ratio of pGSK3β/GSK3β in the COX10 nKO (Fig. 4C). This phosphorylation and inactivation of GSK3β coincide with the onset of the mitochondrial defect. Interestingly, as disease progresses, there is a switch in GSK3 activity passing from an inactive to an active form in the nKO mice. To confirm this switch in activity, we examined the phosphorylation of glycogen synthase (GS), a known substrate of the GSK3. Figure 4D shows that phosphorylation of GS (pGS) at 2 months is very low, which is in agreement with an inactive GSK3. However, at 3 months, there was a significant decrease in the levels of GS and there was a significant increase in pGS at Ser641, confirming the activation of GSK3 in the nKO mice at this age. We observed similar results in hippocampus homogenates of 3-month-old nKO mice, indicating activation of GSK3 (Supplemental Material, Fig. S7).

Discussion

In the present study, we investigated early metabolic adaptations in a mouse model of mitochondria encephalopathy caused by cytochrome oxidase deficiency. As observed in previous COX10 conditional KO mouse models (liver and muscle) (5,39,40), the onset of the mitochondrial defect in the COX10 nKO did not trigger immediate cell death. More specifically, the COX-deficient neurons were able to survive from the onset of mitochondrial defect, at 1–2 months, to the first signs of neurodegeneration, at 4 months (5), suggesting the presence of metabolic adaptations to sustain neuronal survival.

Brain energy metabolism is a complex and still controversial process. The adult brain uses glucose as its primary source of energy and consumes about 20% of the total body glucose. In 1994, a metabolic coupling between astrocytes and neurons was proposed [astrocyte-neuron-lactate shuttle (ANLS)] (41). The ANLS hypothesis proposed that the glutamate released from synaptic terminals is taken up by astrocytes, stimulating glucose consumption in these cells. During glycolysis, astrocytes produce lactate, which is transported outside the cell (via MCT1) and is taken up by the neurons (via MCT2). Neurons metabolize lactate to pyruvate, which enters the TCA cycle and produces ATP through the mitochondrial OXPHOS system. This concept has been challenged over the years and newer evidence indicates that neurons are not only oxidative as proposed by the ANLS hypothesis but they are also capable to carry out glycolysis (13) and can even synthesize glycogen (42).

We observed an increase in glucose uptake, glycolytic intermediates, increased HK and PK enzymatic activity and increased LDHA expression (LDH5 and LDH4) in cortical and hippocampal homogenates of COX10 nKO mice, all supportive of an increased glycolytic metabolism. In addition, intermediates of the PPP were increased, suggesting that the excess of glucose uptake was also diverted to this pathway. More importantly, the increase in glycolysis was able to efficiently maintain the energetic demands of the respiratory deficient brain as the ATP levels in COX10 nKO mice were no different from the ones in control mice. Metabolic abnormalities have been observed in patients with mitochondrial encephalopathies. Proton nuclear magnetic resonance spectroscopy (^{1}H-MRS) revealed elevated levels of lactate in brains of patients with LS or with mitochondrial encephalomyopathy with lactic acidosis and stroke-like episodes, indicative of a switch to a glycolytic metabolism (43). However, these changes are not specific to mitochondrial diseases and have been observed in stroke or seizures. Previous studies showed a decrease in brain 2[^{18}F]fluoro-deoxyglucose uptake, detected by positron emission tomography, in patients with mitochondrial diseases with or without CNS involvement (44). The alteration in glucose uptake did not appear to be related to defects in the vasculature but rather to cytopathies affecting neurons and glia (44). In the COX10 nKO mice, the global metabolomic analysis indicated elevated levels of lactate, confirming our previous ^{1}H-MRS studies (5) and the observations in patients. Similar increases in lactate production were also reported in the mutator mouse (45). The mutator mouse is a knock-in expressing a proofreading-deficient mitochondrial DNA (mtDNA) polymerase that causes the accumulation of deletions and point mutations in the mtDNA. The accumulation of mtDNA mutations in this mouse model causes mitochondrial dysfunction and a premature progeroid phenotype. The increased brain lactate in the mutator mouse was attributed to a switch in the transcription of LDHB to LDHA, favoring the pyruvate to lactate reaction (45). These results support our findings of higher levels of LDH4 and LDH5 in the COX10 nKO mouse.

Metabolomic analysis of brain tissue of another mitochondrial encephalopathy mouse model resembling LS also showed

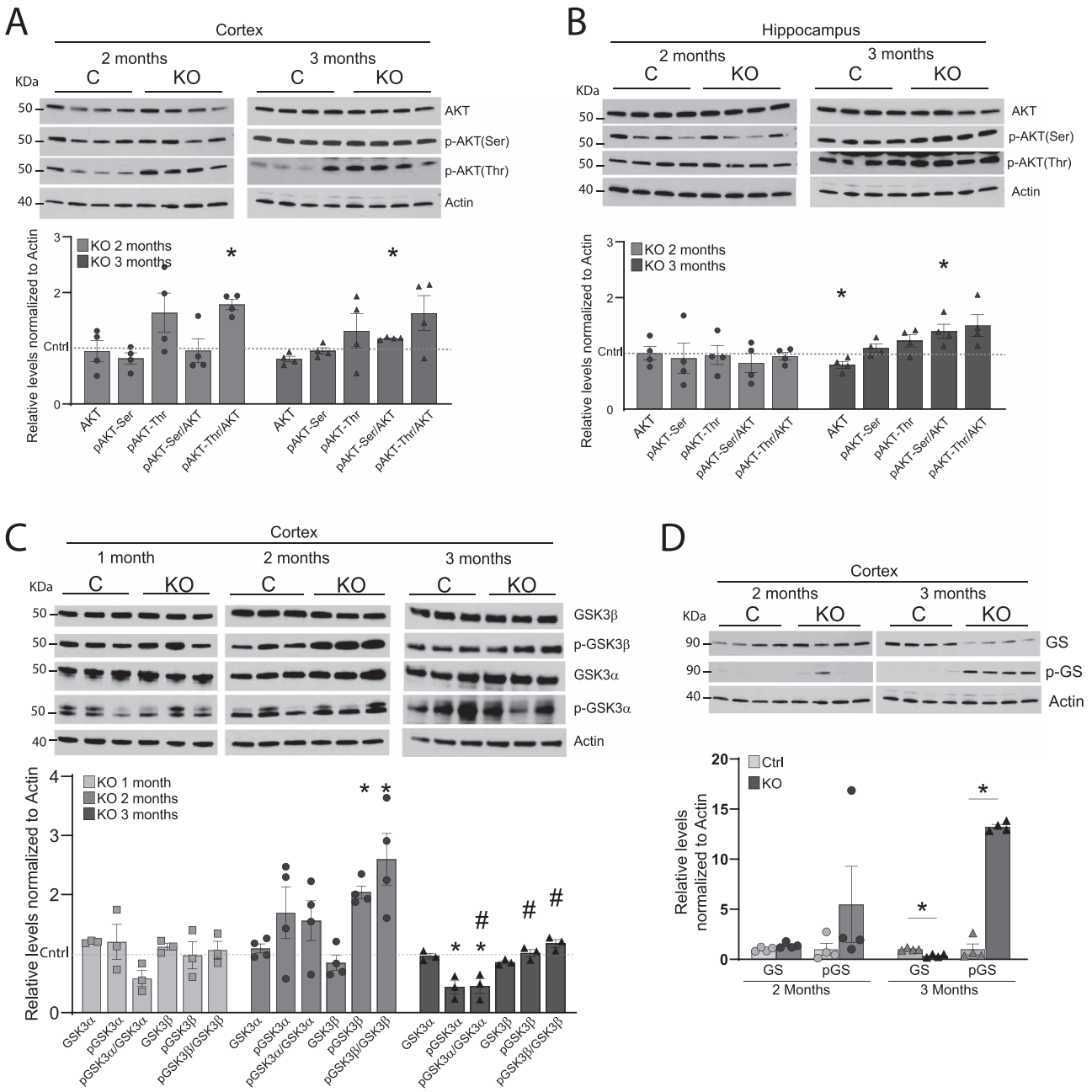

Figure 4. AKT and GSK3 phosphorylation in the COX10 nKO. Western blots of cortex (**A**) and hippocampus (**B**) homogenates of control and nKO mice at 2 and 3 months using antibodies against total AKT and phosphorylation in Thr308 and Ser473 residues. The increase in the levels of pAKT/AKT suggests activation of this kinase. Graphs showed quantification of western blots represented by mean and standard deviation of values normalized to the loading control actin ($n = 4$). (**C**) Western blots of cortex homogenates at different ages of control and nKO mice with antibodies for GSK3 isoforms and the phosphorylated protein in Ser21 and Ser9 for GSK3α and GSK3β, respectively. (**D**) Western blot of glycogen synthase and the phosphorylated form in control and nKO mice at 2 and 3 months and quantification of levels relative to the loading control ($n = 4$). GS is a target of GSK3 and its increase in phosphorylation at 3 months confirms activation of GSK3. (*) indicates $P < 0.05$.

an increase in glycolytic intermediates in 30-day-old mice when the levels of ATP were comparable to control values (46). The LS mouse model was created by the deletion of Ndufs4, a complex I subunit. A switch in the metabolism with increased glycolysis observed in the Ndufs4 KO mice is similar to our results in the COX10 nKO mice, however, the mechanism appears to be different. In the Ndufs4 KO mice, there was an increase in the steady-state levels of HK (46), but this was not the case in our COX10 nKO mice. We observed an increase in the enzymatic activity rather than changes on the steady-steady state levels of HK, supporting the importance of post-translational modifications. An activation of the mTOR pathway has been observed in the Ndufs4 KO mouse and treatment with rapamycin normalized the metabolomics profile, ameliorated pathological phenotype and extended lifespan of the CI-deficient mice (46).

Our findings on alterations of the phosphoproteome led us to investigate the main kinases involved in cell metabolism and survival. Changes in the metabolism and cell survival correlated with activation of the AKT-GSK3 signaling pathway in the COX10 nKO mice. At the onset of the mitochondrial defect, we observed

a significant phosphorylation/inactivation of GSK3, presumably by AKT. Inhibition of GSK3 by phosphorylation at either Ser21 or Ser9 for GSK3α and β, respectively, protects neurons from different adverse stimulus. Activation of GSK3 has been associated with various neurodegenerative disorders (38). Inhibition of GSK3 using the reversible inhibitor lithium resulted to be neuroprotective in pre-clinical models of Amyotrophic Lateral Sclerosis, Alzheimer's, Huntington's and Parkinson's diseases (47). The protective mechanism of GSK3 inhibition has been proposed to be owing to an increased association of hexokinase 2 (HK2) with the mitochondrial outer membrane through binding with the voltage-dependent anion channel (VDAC), which prevents the interaction of the proapoptotic molecules, Bad and Bax, with the mitochondria (48). Association of HK2 to the mitochondria promotes glycolysis (49). When GSK3 is active, it phosphorylates VDAC and disrupts its interaction with HK2. The dissociation of HK2 leads to permeability transition pore formation and subsequent apoptosis (50,51).

This adaptive neuroprotective mechanism that inactivated GSK3 in the COX10 nKO mice is not long-lasting and, at 3 months, there is a switch from an inactive to an active GSK3. We hypothesize that, at a certain point, glucose utilization is not enough to rescue the defect and that the adaptive response is blunted. The latter activation of GSK3 contributes to a delayed neurodegeneration of the respiratory deficient neurons by 4 months. It will be important to further test this hypothesis and determine if prolonging the inhibition of GSK3 will delay neuronal death while maintaining the energetic needs of the neurons.

The impaired mitochondrial function in the COX10 nKO mice also altered lipid metabolism, and the metabolomics analysis revealed the accumulation of phospholipid precursors (phosphocholine and phosphoethanolamine), lysolipids and also lipid degradation products (glycerophosphocholine, glycerophosphoethanolamine and sphingosine). The changes observed in the COX10 nKO mice in the lipids are suggestive of metabolism and remodeling of cellular membrane producing various types of lysolipids (52). Lysolipids act as signaling molecules and are known to interact with G-protein couple receptors (53). One of these molecules is the sphingosine-1-phosphate (S1P), which is formed by the phosphorylation of sphingosine. Among many of the cellular processes that are involved, SP1 promotes cell survival by blocking ceramide-dependent apoptosis (54). The metabolomic analysis did not detected S1P, however, the levels of its precursor sphingosine were significantly increased in cortex and hippocampus in the 3-month-old COX10 nKOs. The implications of the altered lipid metabolism and lipid signaling in the mitochondrial-deficient mouse model warrant further investigation but were beyond the scope of this study.

In summary, we have identified early adaptive responses to neurons under mitochondrial stress that involved an enhancement in glycolytic metabolism. Post-translational modifications, rather than changes in the steady-state level of glycolytic enzymes, were observed in the COX10 nKO. We identified GSK3 as a key mediator of the metabolic changes enhancing glycolysis and promoting neuronal survival in the mitochondrial defective mouse. Modulating GSK3 activity could result beneficial for the treatment of mitochondrial diseases.

Material and Methods

Animal husbandry

In this study, we used our COX-deficient encephalopathy mouse model, the COX10 nKO mouse described earlier (5,6). Mice were fed *ad libitum* with standard chow and were kept in a pathogen-free facility. All procedures performed in mice were approved by the University of Miami IACUC committee.

Western blot analysis of cortex and hippocampus homogenates

Mice were perfused transcardially with cold PBS to remove blood, brain tissue (cortex and hippocampus) dissected, flash-frozen in liquid nitrogen and stored at −80°C until use. Homogenates were prepared by resuspending frozen tissue in PBS containing Complete Protease Inhibitors Cocktail and PhosSTOP (Roche) and by grinding the tissue with an eppendorf teflon pestle until homogeneous (10–15 strokes). Then samples were centrifuged at 1000 rpm for 5 min and the supernatant was used for various assays. Protein concentrations were determined using the DC Bradford reagent from Bio-Rad and the proteins were separated by SDS-PAGE using pre-cast 4–20% acrylamide gels (Bio-Rad). Proteins were then transferred to PVDF or nitrocellulose membranes and were immunodecorated with various antibodies. Signal from secondary antibody was developed with West Pico Super Signal ECL from Pierce or with Clarity ECL from Bio-Rad by using film. Primary antibodies used include: hexokinase1, pyruvate kinase m2, phosphor-pyruvate kinase m2, PDK1, phosphofructokinase 2, glyceraldehyde-3-phosphate dehydrogenase, enolase 2, lactate dehydrogenase A, phospho-lactate dehydrogenase A, pyruvate dehydrogenase, glutamate dehydrogenase, GSK3α and β and pGSK3α and β, glycogen synthase, phosphoglycogen synthase, AMPK, pAMPKa, AKT pAKT(ser), phospho-AKT-Threo (Cell signaling), actin and tubulin (Sigma), MCT1 (Millipore) and MCT2 (Santa Cruz).

Metabolomic analysis of brain tissue

Cortexes or hippocampuses of 2- and 3-month-old control and nKO mice ($n = 8$ for each group) were quickly dissected from mice and were immediately frozen in liquid nitrogen. Frozen samples were sent to Metabolon Inc (Durham, NC) for processing and analysis. For sample preparation, they added recovery standards for QC purposes prior to the first step of extraction with a proprietary series of organic and aqueous extractions that removed the protein fraction and allowed for a maximum recovery of small molecules. The resulting extracts were divided into two fractions; one for analysis by LC and one for analysis by GC. Organic solvents were removed in a TurboVap® (Zymark) and samples were frozen and dried under vacuum. Samples were then prepared for the appropriate instrument, either by LC/MS or by GC/MS. For the LC/MS and LC/MSMS platforms, Waters ACQUITY UPLC and Thermo-Finnigan LTQ mass spectrometers were used, respectively. For GC/MS, samples were analyzed on a Thermo-Finnigan Trace DSQ fast-scanning single-quadrupole mass spectrometer using electron impact ionization. Compounds were identified by comparison to library entries of purified standards or recurrent unknown entities. Identification of known chemical entities was based on comparison to metabolomic library entries (>1000) of purified standards. Data normalization step was performed to correct variation resulting from instrument inter-day tuning differences. Statistical analysis of two-way ANOVA and false discovery rate were performed. Results obtained from Metabolon Inc showing fold differences are shown in Supplemental Material, Tables S1 and S2. A $P \leq 0.05$ is considered to be statistically significant. Heat maps were generated using MetaboAnalyst 5.0. Peak Intensity values were

uploaded for selected metabolites. Data were normalized to median values and no QC data filtering was performed.

Determination of glucose uptake in the brain

Mice were starved for 6–7 h and were then injected i.p. with 100 μl of saline solution containing 2 μCi of [^{14}C]2-DG (specific activity: 250–350 mCi/mmol, Perkin Elmer). Forty-five minutes after the injection, mice were sacrificed, brain was removed and frozen in liquid nitrogen vapors. Serial brain slices of 25 μm were obtained in a cryostat, mounted on glass coverslip and exposed to BioMax MR Kodak film along with [^{14}C]methylmethacrylate standards for 10 days, as described in (55,56). Images obtained by film exposure were digitalized by using a CCD camera and an image analysis system software (MCID, Image research Canada).

Determination of the enzymatic activity of glycolytic enzymes

Enzymatic activities were measured spectrophotometrically following the oxidation of NADH in cortex homogenates in a Beckman spectrophotometer. Homogenates (about 10% w/v) were prepared in 20 mM potassium phosphate buffer pH 8.0 and centrifuged at 10 000 $\times g$ for 10 min. The supernatant was diluted with three volumes of 20 mM NaFl and 1 mM mM EDTA and complete protease inhibitors cocktail (Roche). PFK activity was measured in 40 mM Tris–HCl pH 8.0 containing 6 mM $MgCl_2$, 2 mM ATP, 0.2 mM NADH, five units of glycerophosphate dehydrogenase triosephosphate isomerase (Sigma G1881), 1.5 units of aldolase (Sigma A8811) and enzyme (homogenate) final concentration in a total volume of 1 ml. The reaction was initiated with 3 mM fructose-6-phosphate, and NADH oxidation was measured by absorbance at 340 nm at 30°C for about 3 min (Layzer 1967).

LDH activity was measured in a mixture containing 30 mM potassium phosphate pH 7.4, 3 mM pyruvate, 0.4 mM NADH, 1 mM NaCl and homogenate in a final volume of 1 ml. Reaction was initiated with homogenate and followed absorbance at 340 nm. The HK activity was measured in a mixture containing 50 mM Hepes pH 7.8, 100 mM KCl, 7.5 mM $MgCl_2$, 5 mM dithiotreitol, 0.5 mM NAD+, 5 mM glucose, one unit of glucose 6-phosphate dehydrogenase from *Leuconostoc mesenteroides* (Sigma G5885) and 2.5 mM ATP final concentration in a total volume of 1 ml (Agius and Torch 1990). Assay was performed at 30°C and absorbance was measured at 340 nm after starting reaction with ATP.

PK was measured in 100 mM Tris–HCl pH 7.4, 2.5 mM $MgCl_2$, 10 mM KCl, 0.5 mM phosphoenolpyruvate, 5 mM ADP, 0.2 mM NADH and 15 units of LDH (Sigma L2625) in a final volume of 1 ml (Bergmeyer 1974). The reaction was started with the homogenates and absorbance followed at 340 nm at 30°C.

Proteomic analysis by two-dimensional differential gel electrophoresis

Two-dimensional differential gel electrophoresis and MS were performed by Applied Biomics (Hayward, CA). Frozen tissues (20 mg) were resuspended in 200 μl of 2-D cell lysis buffer (30 mM Tris–HCl, pH 8.8, 7 M urea, 2 M thiourea and 4% CHAPS), sonicated at 4°C and incubated for 30 min at room temperature in shaker. Samples were centrifuged at 20 000 $\times g$ for 30 min and protein concentration was determined in the supernatant and was diluted to 6 mg/ml in 2-D cell lysis buffer. Proteins (30 μg) were labeled with 1 μl of 0.2 nmol/μl CyDye (either Cy3 or Cy5) diluted in DMF for 30 min on ice protected from light, then 1 μl of 10 mM lysine was added, sample vortexed and incubated for 15 min. Samples from control and nKO mice labeled with Cy3 or Cy5, respectively, were mixed. Then 2X 2-D sample buffer (8 M urea, 4% CHAPS, 20 mg/ml DTT, 2% pharmalytes and trace amount of bromophenol blue) and 100 μl of DeStreak™ solution and rehydration buffer (7 M urea, 2 M thiourea, 4% CHAPS, 20 mg/ml DTT, 1% pharmalytes and trace amount of bromophenol blue) were added to a final volume of 250 μl. Samples were loaded into strip holder of 13 cm IPG strips (Amersham Biosciences). Proteins were separated by isoelectric focusing according to manufacturer's specifications in the dark at 20°C. Then, IPG strips were equilibrated in buffer 1 (50 mM Tris–HCl, pH 8.8, containing 6 M urea, 30% glycerol, 2% SDS, trace amount of bromophenol blue and 10 mg/ml DTT) for 15 min. Then, strips were incubated in equilibration buffer 2 (50 mM Tris–HCl, pH 8.8, containing 6 M urea, 30% glycerol, 2% SDS, trace amount of bromophenol blue and 45 mg/ml Iodacetamide) for 10 min. IPG strips were then rinsed once in the SDS-gel running buffer before placing them into a 12% SDS-PAGE for the second dimension. Fluorescent proteins in the 2-D gels were detected using the Typhoon TRIO scanner (GE Healthcare) following the protocols manufacturer's instructions. The scanned images were then analyzed by Image QuantTL software (GE Healthcare) and then subjected to in-gel analysis and cross-gel analysis using DeCyder software version 6.5 (GE Healthcare). The ratio change of the protein differential expression was obtained from in-gel DeCyder software analysis. To detect phosphorylated proteins, the 2-D gels were stained with ProQ diamond phospho-protein staining kit (Invitrogen) and were also scanned as indicated before.

Protein identification by MS

The spots of interest were picked up using the Ettan Spot Picker (GE Healthcare) based on the in-gel analysis and spot-picking design by the DeCyder software. Gel spots were washed and digested in-gel with modified porcine trypsin protease (Trypsin Gold, Promega). The tryptic peptides obtained were desalted using Zip-tip C18 (Millipore) tips and eluted from with 0.5 μl of matrix solution (α-cyano-4-hydroxycinnamic acid, 5 mg/ml in 50% acetonitrile, 0.1% trifluoroacetic acid and 25 mM ammonium bicarbonate). Samples were spotted on the MALDI plate. MALDI-TOF (MS) and TOF/TOF (tandem MS/MS) were performed on a 5800 mass spectrometer (AB Sciex). MALDI-TOF mass spectra were acquired in reflectron positive ion mode, averaging 2000 laser shots per spectrum. TOF/TOF tandem MS fragmentation spectra were acquired for each sample, averaging 2000 laser shots per fragmentation spectrum on each of the 5–10 most abundant ions present in each sample (excluding trypsin autolytic peptides and other known background ions). Both the resulting peptide mass and the associated fragmentation spectra were submitted to GPS Explorer version 3.5 equipped with MASCOT search engine (Matrix science) to search the database of National Center for Biotechnology Information non-redundant. Searches were performed without constraining protein molecular weight or isoelectric point, with variable carbamidomethylation of cysteine and oxidation of methionine residues and with one missed cleavage allowed in the search parameters. Candidates with either protein score C.I.% or Ion C.I.% >95 were considered to be significant.

Statistical analysis

Statistical significance was determined using unpaired Student *t*-test to compare two groups. A $P < 0.05$ was considered to be

statistically significant. Western blot signals in film were scanned and quantified by densitometry using Image J software. Signals were normalized to loading controls, such as actin or tubulin signals, obtained in the same membrane.

Supplementary Material

Supplementary Material is available at *HMG* online.

Acknowledgements

We would like to thank Ofelia Alonso Quinones and Dr Helen Bramlett, for assistance with the 2-DG experiments, and Jose A. Oca and Dr Susana Peralta, for critical review of the manuscript.

Conflict of Interest statement. None declared.

Funding

F.D.'s research has been supported by the James and Esther King Research Program Florida Department of Health (grant 08KN-01), the National Institute of Health (grant GM101225) and the United Mitochondrial Disease Foundation (grant 14050R). C.T.M.'s research was supported by NIH grants R01NS079965 and R01EY010804, the James and Esther King Research Program Florida Department of Health (grant 21 K05) and the Army Research Office grant W911NF.

Authors' contributions

Conceptualization was by C.T.M and F.D.; methodology was by A.P.R., C.T.M. and F.D.; investigation was by S.G., A.S.-C., M.A., A.P.R. and F.D.; writing of the original draft was by F.D.; review and editing were performed by S.G., A.S.-C., A.P.R., N.N., M.P., C.T.M. and F.D.; supervision was by C.T.M. and F.D.

References

1. Gorman, G.S., Schaefer, A.M., Ng, Y., Gomez, N., Blakely, E.L., Alston, C.L., Feeney, C., Horvath, R., Yu-Wai-Man, P., Chinnery, P.F. *et al.* (2015) Prevalence of nuclear and mitochondrial DNA mutations related to adult mitochondrial disease. *Ann. Neurol.*, **77**, 753–759.
2. Iommarini, L., Peralta, S., Torraco, A. and Diaz, F. (2015) Mitochondrial Diseases Part II: mouse models of OXPHOS deficiencies caused by defects in regulatory factors and other components required for mitochondrial function. *Mitochondrion*, **22**, 96–118.
3. Torraco, A., Peralta, S., Iommarini, L. and Diaz, F. (2015) Mitochondrial Diseases Part I: mouse models of OXPHOS deficiencies caused by defects in respiratory complex subunits or assembly factors. *Mitochondrion*, **21**, 76–91.
4. Lin, M.T. and Beal, M.F. (2006) Mitochondrial dysfunction and oxidative stress in neurodegenerative diseases. *Nature*, **443**, 787–795.
5. Diaz, F., Garcia, S., Padgett, K.R. and Moraes, C.T. (2012) A defect in the mitochondrial complex III, but not complex IV, triggers early ROS-dependent damage in defined brain regions. *Hum. Mol. Genet.*, **21**, 5066–5077.
6. Fukui, H., Diaz, F., Garcia, S. and Moraes, C.T. (2007) Cytochrome c oxidase deficiency in neurons decreases both oxidative stress and amyloid formation in a mouse model of Alzheimer's disease. *Proc. Natl. Acad. Sci. U. S. A.*, **104**, 14163–14168.
7. Fontanesi, F., Soto, I.C., Horn, D. and Barrientos, A. (2006) Assembly of mitochondrial cytochrome c-oxidase, a complicated and highly regulated cellular process. *Am. J. Physiol. Cell Physiol.*, **291**, C1129–C1147.
8. Mogi, T., Saiki, K. and Anraku, Y. (1994) Biosynthesis and functional role of haem O and haem A. *Mol. Microbiol.*, **14**, 391–398.
9. Nobrega, M.P., Nobrega, F.G. and Tzagoloff, A. (1990) COX10 codes for a protein homologous to the ORF1 product of *Paracoccus denitrificans* and is required for the synthesis of yeast cytochrome oxidase. *J. Biol. Chem.*, **265**, 14220–14226.
10. Antonicka, H., Leary, S.C., Guercin, G.H., Agar, J.N., Horvath, R., Kennaway, N.G., Harding, C.O., Jaksch, M. and Shoubridge, E.A. (2003) Mutations in COX10 result in a defect in mitochondrial heme A biosynthesis and account for multiple, early-onset clinical phenotypes associated with isolated COX deficiency. *Hum. Mol. Genet.*, **12**, 2693–2702.
11. Coenen, M.J., van den Heuvel, L.P., Ugalde, C., Ten Brinke, M., Nijtmans, L.G., Trijbels, F.J., Beblo, S., Maier, E.M., Muntau, A.C. and Smeitink, J.A. (2004) Cytochrome c oxidase biogenesis in a patient with a mutation in COX10 gene. *Ann. Neurol.*, **56**, 560–564.
12. Valnot, I., von Kleist-Retzow, J.C., Barrientos, A., Gorbatyuk, M., Taanman, J.W., Mehaye, B., Rustin, P., Tzagoloff, A., Munnich, A. and Rotig, A. (2000) A mutation in the human heme A: farnesyltransferase gene (COX10) causes cytochrome c oxidase deficiency. *Hum. Mol. Genet.*, **9**, 1245–1249.
13. Lundgaard, I., Li, B., Xie, L., Kang, H., Sanggaard, S., Haswell, J.D., Sun, W., Goldman, S., Blekot, S., Nielsen, M. *et al.* (2015) Direct neuronal glucose uptake heralds activity-dependent increases in cerebral metabolism. *Nat. Commun.*, **6**, 6807.
14. Pierre, K. and Pellerin, L. (2005) Monocarboxylate transporters in the central nervous system: distribution, regulation and function. *J. Neurochem.*, **94**, 1–14.
15. Simpson, I.A., Carruthers, A. and Vannucci, S.J. (2007) Supply and demand in cerebral energy metabolism: the role of nutrient transporters. *J. Cereb. Blood Flow Metab.*, **27**, 1766–1791.
16. Leino, R.L., Gerhart, D.Z. and Drewes, L.R. (1999) Monocarboxylate transporter (MCT1) abundance in brains of suckling and adult rats: a quantitative electron microscopic immunogold study. *Brain Res. Dev. Brain Res.*, **113**, 47–54.
17. Pierre, K., Debernardi, R., Magistretti, P.J. and Pellerin, L. (2003) Noradrenaline enhances monocarboxylate transporter 2 expression in cultured mouse cortical neurons via a translational regulation. *J. Neurochem.*, **86**, 1468–1476.
18. Tamada, M., Suematsu, M. and Saya, H. (2012) Pyruvate kinase M2: multiple faces for conferring benefits on cancer cells. *Clin. Cancer Res.*, **18**, 5554–5561.
19. Hitosugi, T., Kang, S., Vander Heiden, M.G., Chung, T.W., Elf, S., Lythgoe, K., Dong, S., Lonial, S., Wang, X., Chen, G.Z. *et al.* (2009) Tyrosine phosphorylation inhibits PKM2 to promote the Warburg effect and tumor growth. *Sci. Signal.*, **2**, ra73.
20. Ashizawa, K., Willingham, M.C., Liang, C.M. and Cheng, S.Y. (1991) In vivo regulation of monomer-tetramer conversion of pyruvate kinase subtype M2 by glucose is mediated via fructose 1,6-bisphosphate. *J. Biol. Chem.*, **266**, 16842–16846.
21. Shepherd, R.K., Checcarelli, N., Naini, A., De Vivo, D.C., DiMauro, S. and Sue, C.M. (2006) Measurement of ATP

production in mitochondrial disorders. *J. Inherit. Metab. Dis.*, **29**, 86–91.
22. Biagioli, M., Pinto, M., Cesselli, D., Zaninello, M., Lazarevic, D., Roncaglia, P., Simone, R., Vlachouli, C., Plessy, C., Bertin, N. *et al.* (2009) Unexpected expression of alpha- and beta-globin in mesencephalic dopaminergic neurons and glial cells. *Proc. Natl. Acad. Sci. U. S. A.*, **106**, 15454–15459.
23. Richter, F., Meurers, B.H., Zhu, C., Medvedeva, V.P. and Chesselet, M.F. (2009) Neurons express hemoglobin alpha- and beta-chains in rat and human brains. *J. Comp. Neurol.*, **515**, 538–547.
24. Schelshorn, D.W., Schneider, A., Kuschinsky, W., Weber, D., Kruger, C., Dittgen, T., Burgers, H.F., Sabouri, F., Gassler, N., Bach, A. *et al.* (2009) Expression of hemoglobin in rodent neurons. *J. Cereb. Blood Flow Metab.*, **29**, 585–595.
25. Baba, T., Kobayashi, H., Kawasaki, H., Mineki, R., Naito, H. and Ohmori, D. (2010) Glyceraldehyde-3-phosphate dehydrogenase interacts with phosphorylated Akt resulting from increased blood glucose in rat cardiac muscle. *FEBS Lett.*, **584**, 2796–2800.
26. Agius, L. (2015) Role of glycogen phosphorylase in liver glycogen metabolism. *Mol. Asp. Med.*, **46**, 34–45.
27. Mihaylova, M.M. and Shaw, R.J. (2011) The AMPK signalling pathway coordinates cell growth, autophagy and metabolism. *Nat. Cell Biol.*, **13**, 1016–1023.
28. Hardie, D.G., Ross, F.A. and Hawley, S.A. (2012) AMPK: a nutrient and energy sensor that maintains energy homeostasis. *Nat. Rev. Mol. Cell Biol.*, **13**, 251–262.
29. Merrill, G.F., Kurth, E.J., Hardie, D.G. and Winder, W.W. (1997) AICA riboside increases AMP-activated protein kinase, fatty acid oxidation, and glucose uptake in rat muscle. *Am. J. Phys.*, **273**, E1107–E1112.
30. Marsin, A.S., Bertrand, L., Rider, M.H., Deprez, J., Beauloye, C., Vincent, M.F., Van den Berghe, G., Carling, D. and Hue, L. (2000) Phosphorylation and activation of heart PFK-2 by AMPK has a role in the stimulation of glycolysis during ischaemia. *Curr. Biol.*, **10**, 1247–1255.
31. Manning, B.D. and Cantley, L.C. (2007) AKT/PKB signaling: navigating downstream. *Cell*, **129**, 1261–1274.
32. Risso, G., Blaustein, M., Pozzi, B., Mammi, P. and Srebrow, A. (2015) Akt/PKB: one kinase, many modifications. *Biochem. J.*, **468**, 203–214.
33. Alessi, D.R., James, S.R., Downes, C.P., Holmes, A.B., Gaffney, P.R., Reese, C.B. and Cohen, P. (1997) Characterization of a 3-phosphoinositide-dependent protein kinase which phosphorylates and activates protein kinase B alpha. *Curr. Biol.*, **7**, 261–269.
34. Sarbassov, D.D., Guertin, D.A., Ali, S.M. and Sabatini, D.M. (2005) Phosphorylation and regulation of Akt/PKB by the rictor-mTOR complex. *Science*, **307**, 1098–1101.
35. Ruggero, D. and Sonenberg, N. (2005) The Akt of translational control. *Oncogene*, **24**, 7426–7434.
36. Woodgett, J.R. (2005) Recent advances in the protein kinase B signaling pathway. *Curr. Opin. Cell Biol.*, **17**, 150–157.
37. Yung, H.W., Charnock-Jones, D.S. and Burton, G.J. (2011) Regulation of AKT phosphorylation at Ser473 and Thr308 by endoplasmic reticulum stress modulates substrate specificity in a severity dependent manner. *PLoS One*, **6**, e17894.
38. Eldar-Finkelman, H. (2002) Glycogen synthase kinase 3: an emerging therapeutic target. *Trends Mol. Med.*, **8**, 126–132.
39. Diaz, F., Garcia, S., Hernandez, D., Regev, A., Rebelo, A., Oca-Cossio, J. and Moraes, C.T. (2008) Pathophysiology and fate of hepatocytes in a mouse model of mitochondrial hepatopathies. *Gut*, **57**, 232–242.
40. Diaz, F., Thomas, C.K., Garcia, S., Hernandez, D. and Moraes, C.T. (2005) Mice lacking COX10 in skeletal muscle recapitulate the phenotype of progressive mitochondrial myopathies associated with cytochrome c oxidase deficiency. *Hum. Mol. Genet.*, **14**, 2737–2748.
41. Pellerin, L. and Magistretti, P.J. (1994) Glutamate uptake into astrocytes stimulates aerobic glycolysis: a mechanism coupling neuronal activity to glucose utilization. *Proc. Natl. Acad. Sci. U. S. A.*, **91**, 10625–10629.
42. Lopez-Ramos, J.C., Duran, J., Gruart, A., Guinovart, J.J. and Delgado-Garcia, J.M. (2015) Role of brain glycogen in the response to hypoxia and in susceptibility to epilepsy. *Front. Cell. Neurosci.*, **9**, 431.
43. Saneto, R.P., Friedman, S.D. and Shaw, D.W. (2008) Neuroimaging of mitochondrial disease. *Mitochondrion*, **8**, 396–413.
44. Molnar, M.J., Valikovics, A., Molnar, S., Tron, L., Dioszeghy, P., Mechler, F. and Gulyas, B. (2000) Cerebral blood flow and glucose metabolism in mitochondrial disorders. *Neurology*, **55**, 544–548.
45. Ross, J.M., Oberg, J., Brene, S., Coppotelli, G., Terzioglu, M., Pernold, K., Goiny, M., Sitnikov, R., Kehr, J., Trifunovic, A. *et al.* (2010) High brain lactate is a hallmark of aging and caused by a shift in the lactate dehydrogenase A/B ratio. *Proc. Natl. Acad. Sci. U. S. A.*, **107**, 20087–20092.
46. Johnson, S.C., Yanos, M.E., Kayser, E.B., Quintana, A., Sangesland, M., Castanza, A., Uhde, L., Hui, J., Wall, V.Z., Gagnidze, A. *et al.* (2013) mTOR inhibition alleviates mitochondrial disease in a mouse model of Leigh syndrome. *Science*, **342**, 1524–1528.
47. Forlenza, O.V., De-Paula, V.J. and Diniz, B.S. (2014) Neuroprotective effects of lithium: implications for the treatment of Alzheimer's disease and related neurodegenerative disorders. *ACS Chem. Neurosci.*, **5**, 443–450.
48. Gimenez-Cassina, A., Lim, F., Cerrato, T., Palomo, G.M. and Diaz-Nido, J. (2009) Mitochondrial hexokinase II promotes neuronal survival and acts downstream of glycogen synthase kinase-3. *J. Biol. Chem.*, **284**, 3001–3011.
49. John, S., Weiss, J.N. and Ribalet, B. (2011) Subcellular localization of hexokinases I and II directs the metabolic fate of glucose. *PLoS One*, **6**, e17674.
50. Chiara, F., Castellaro, D., Marin, O., Petronilli, V., Brusilow, W.S., Juhaszova, M., Sollott, S.J., Forte, M., Bernardi, P. and Rasola, A. (2008) Hexokinase II detachment from mitochondria triggers apoptosis through the permeability transition pore independent of voltage-dependent anion channels. *PLoS One*, **3**, e1852.
51. Wilson, J.E. (2003) Isozymes of mammalian hexokinase: structure, subcellular localization and metabolic function. *J. Exp. Biol.*, **206**, 2049–2057.
52. Arouri, A. and Mouritsen, O.G. (2013) Membrane-perturbing effect of fatty acids and lysolipids. *Prog. Lipid Res.*, **52**, 130–140.
53. Tomura, H., Mogi, C., Sato, K. and Okajima, F. (2005) Proton-sensing and lysolipid-sensitive G-protein-coupled receptors: a novel type of multi-functional receptors. *Cell. Signal.*, **17**, 1466–1476.
54. Maceyka, M., Harikumar, K.B., Milstien, S. and Spiegel, S. (2012) Sphingosine-1-phosphate signaling and its role in disease. *Trends Cell Biol.*, **22**, 50–60.

55. Ginsberg, M.D., Zhao, W., Alonso, O.F., Loor-Estades, J.Y., Dietrich, W.D. and Busto, R. (1997) Uncoupling of local cerebral glucose metabolism and blood flow after acute fluid-percussion injury in rats. *Am. J. Phys.*, **272**, H2859–H2868.

56. Passineau, M.J., Zhao, W., Busto, R., Dietrich, W.D., Alonso, O., Loor, J.Y., Bramlett, H.M. and Ginsberg, M.D. (2000) Chronic metabolic sequelae of traumatic brain injury: prolonged suppression of somatosensory activation. *Am. J. Physiol. Heart Circ. Physiol.*, **279**, H924–H931.